Theoret.Appl.Mech. TEOPM7, Vol.40,No.4,pp.469-510, Belgrade 2013*

MODELLING LAMINAR TRANSPORT PHENOMENA IN A CASSON RHEOLOGICAL FLUID FROM AN ISOTHERMAL SPHERE WITH PARTIAL SLIP IN A NON-DARCY POROUS MEDIUM

V.Ramachandra Prasad **A.Subba Rao**

N.Bhaskar Reddy **O. Anwar Bég**

*doi:10.2298/TAM1304469P Math. Subj. Class.: 74S20; 76A05; 76D10; 82D15.

According to: *Tib Journal Abbreviations (C) Mathematical Reviews*, the abbreviation TEOPM7 stands for TEORIJSKA I PRIMENJENA MEHANIKA.

Theoret. Appl. Mech., Vol.40, No.4, pp. 469–510, Belgrade 2013

Modelling laminar transport phenomena in a Casson rheological fluid from an isothermal sphere with partial slip in a non-Darcy porous medium

V.Ramachandra Prasad [*] **A.Subba Rao** [†]
N.Bhaskar Reddy [‡] **O. Anwar Bég** [§]

Abstract

The flow and heat transfer of Casson fluid from a permeable isothermal sphere in the presence of slip condition in a non-Darcy porous medium is analyzed. The sphere surface is maintained at a constant temperature. The boundary layer conservation equations, which are parabolic in nature, are normalized into non-similar form and then solved numerically with the well-tested, efficient, implicit, stable Keller-box finite-difference scheme. Increasing the velocity slip parameter is found to decrease the velocity and boundary layer thickness and increases the temperature and the boundary layer thickness. The velocity decreases with the increase the non-Darcy parameter and is found to increase the temperature. The velocity increases with the increase the Casson fluid parameter and is found to decrease the temperature. The Skin-friction coefficient and the local Nusselt number is found to decrease with the increase in velocity and thermal slip parameters respectively.

Keywords: Non-Newtonian fluid mechanics; Casson model; yield stress; Slip condition; Keller-box numerical method; Heat transfer; Skin friction; Nusselt number; Boundary layers; Isothermal Sphere

[*]Department of Mathematics, Madanapalle Institute of Technology and Science, Madanapalle-517325, India
[†]Department of Mathematics, Sri Venkateswara University, Tirupathi-517502, India
[‡]Department of Mathematics, Sri Venkateswara University, Tirupathi-517502, India
[§]Gort Engovation (Propulsion and Biomechanics Research), 15 Southmere Ave., Bradford, BD73NU, UK.

Nomenclature

a - radius of the sphere
C_f - skin friction coefficient
S_f - non-dimensional velocity slip parameter
S_T - non-dimensional thermal slip parameter
f - non-dimensional steam function
g - acceleration due to gravity
Gr - Grashof number
Da - Darcian parameter
$r(x)$ - radial distance from symmetrical axis to surface of the sphere
N_0 - velocity slip factor
K_0 - thermal slip factor
Nu - Local Nusselt number
Pr - Prandtl number
V - the linear (translational) fluid velocity vector
T - temperature
u, v - non-dimensional velocity components along the x- and y-directions, respectively
x - stream wise coordinate
y - transverse coordinate

Greek symbols

α - thermal diffusivity
β - the non-Newtonian Casson parameter
Λ - the local inertial drag coefficient (Forchheimer parameter)
Ω - the coefficient of thermal expansion
Φ - the azimuthal coordinate
η - the dimensionless radial coordinate
μ - dynamic viscosity
ν - kinematic viscosity
θ - non-dimensional temperature
ρ - density
σ - the electrical conductivity
ξ - the dimensionless tangential coordinate
ψ - dimensionless stream function

Subscripts

w conditions on the wall
∞ free stream conditions

1 Introduction

Non-Newtonian transport phenomena arise in many branches of chemical and materials processing engineering. Such fluids exhibit shear-stress-strain relationships which diverge significantly from the Newtonian (Navier-Stokes) model. Most non-Newtonian models involve some form of modification to the momentum conservation equations. These include power- law, thixotropic and viscoelastic fluids [1]. Such rheological models however cannot simulate the microstructural characteristics of many important liquids including polymer

suspensions, liquid crystal melts, physiological fluids, contaminated lubricants, etc.

The flow of non-Newtonian fluids in the presence of heat transfer is an important research area due to its wide use in food processing, power engineering, petroleum production and in many industries for example polymers melt and polymer solutions employed in the plastic processing. Several fluids in chemical engineering, multiphase mixtures, pharmaceutical formulations, china clay and coal in water, paints, synthetic lubricants, salvia, synovial fluid, jams, soups, jellies, marmalades, sewage sludge etc. are non-Newtonian. The constitutive relations for these kinds of fluids give rise to more complex and higher order equations than the Navier-Stokes equations. Considerable progress even through has been made on the topic by using different models of non-Newtonian fluids [2-11].

Transport processes in porous media can involve fluid, heat and mass transfer in single or multi-phase scenarios. Such flows with and without buoyancy effects arise frequently in many branches of chemical engineering and owing to their viscous-dominated nature are generally simulated using the Darcy model. Applications of such flows include chip-based microfluidic chromatographic separation devices [12], dissolution of masses buried in a packed bed [13], heat transfer in radon saturating permeable regimes [14], flows in ceramic filter components of integrated gasification combined cycles (IGCC) [15], separation of carbon dioxide from the gas phase with aqueous adsorbents (water and diethanolamine solution) in micro porous hollow fibre membrane modules [16], and monolithic adsorbent flows consisting of micro-porous zeolite particles embedded in a polyamide matrix [17]. Porous media flow simulations are also critical in convective processes in hygroscopic materials [18], electro remediation in soil decontamination technique wherein an electric field applied to a porous medium generates the migration of ionic species in solution [19], reactive transport in tubular porous media reactors [20], perfusive bed flows [21], gelation of biopolymers in porous media which arise in petroleum recovery and in subsurface heavy metal stabilization [22].

Previous studies indicate that not much has been presented yet regarding Casson fluid. This model [23-25] in fact is a plastic fluid that exhibits shear thinning characteristics and that quantifies yield stress and high shear viscosity. Casson fluid model is reduced to a Newtonian fluid at very high wall shear stresses, when wall stress is much greater than yield stress. This fluid has good approximations for many substances such as biological materials, foams, molten chocolate, cosmetics, nail polish, some particulate suspensions etc. The boundary layer behavior of viscoelastic fluid has technical applications in engineering

such as glass fiber, paper production, manufacture of foods, the aerodynamic extrusion of plastic sheets, the polymer extrusion in a melt spinning process and many others.

The objective of the present paper is to investigate the flow and heat transfer of Casson fluid past an isothermal sphere. Mathematical modeling through equations of continuity and motion leads to a nonlinear differential equation even after employing the boundary layer assumptions. The velocity and thermal slip conditions along with conservation law of mass, momentum and energy completes the problems formulation for velocity components and temperature. The considered slip conditions especially are important in the non-Newtonian fluids such as polymer melts which often exhibit wall slip. It has been experimentally verified that fluid possesses non-continuum features such as slip flow when the molecular mean free path length of fluid is comparable to the distance between the plates as in Nano channels/micro channels [26].

2 Mathematical analysis

A steady, laminar, two-dimensional, viscous, incompressible, electrically - conducting, buoyancy-driven convection heat transfer flow from a permeable isothermal sphere embedded in an isotropic, homogenous, fully-saturated porous medium is considered. Figure 1 illustrates the physical model and coordinate system. Here x is measured along the surface of the sphere, y is measured normal to the surface, respectively and r is the radial distance from symmetric axes to the surface. $R = asin(x/a)$, a is the radius of the sphere. The gravitational acceleration, $\mathbf{g}$ acts downwards. Both the sphere and the fluid are maintained initially at the same temperature. Instantaneously they are raised to a temperature $T_w > T_\infty$, the ambient temperature of the fluid which remains unchanged. The fluid properties are assumed to be constant except the density variation in the buoyancy force term.

The porous medium is simulated using the well tested and validated non-Darcian drag force model. This incorporates a linear Darcian drag for low velocity effects (bulk impedance of the porous matrix at low Reynolds numbers) and a quadratic (second order) resistance, the Forchheimer drag, for high velocity flows, as may be encountered in chemical engineering systems operating at higher velocities. The appropriate non-Darcian model, following Nield and Bejan [27] is therefore:

$$\nabla p = -\frac{\mu}{K}V - \frac{\rho b}{K}V^2 \tag{1}$$

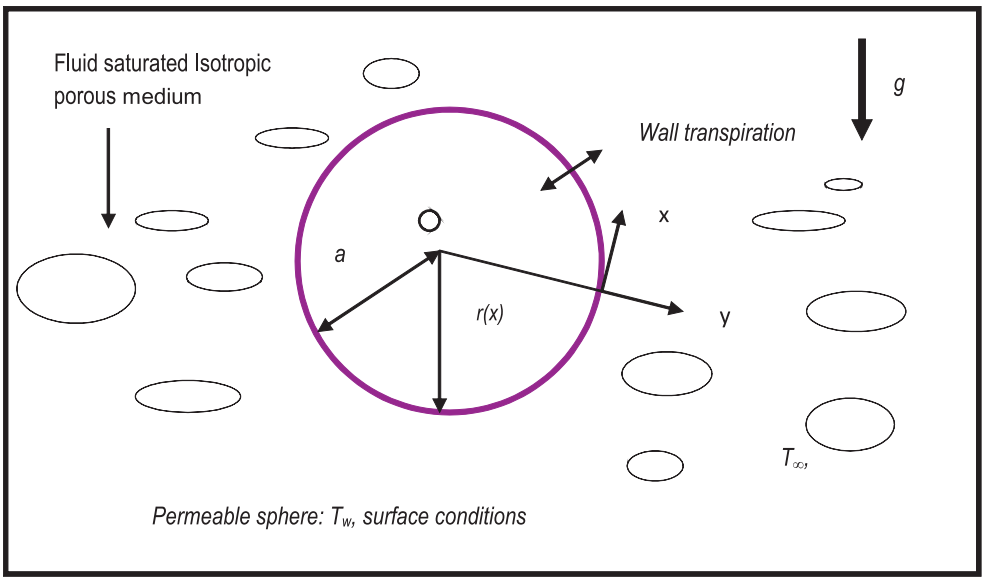

Figure 1: Physical model and coordinate system

where ∇p is the pressure drop across the porous medium μ is the dynamic viscosity of the fluid, b is the Forchheimer (geometric) inertial drag parameter, K is the permeability of the porous medium (hydraulic conductivity) and V is the general velocity.

We also assume the rheological equation of Casson fluid, reported by Mustafa et al. [41] is:

$$\tau^{1/n} = \tau_0^{1/n} + \mu\dot{\gamma}^{1/n} \tag{2}$$

or

$$\tau_{ij} = \left[\mu_B + \left(\frac{P_y}{\sqrt{2\pi}}\right)^{1/n}\right]^n 2e_{ij} \tag{3}$$

where μ is the dynamic viscosity, μ_B the plastic dynamic viscosity of non-Newtonian fluid , $\pi = e_{ij}e_{ij}$ and e_{ij} is the $(i,j)^{th}$ component of deformation rate, π denotes the product of the component of deformation rate with itself, π_c shows a critical value of this product based on the non-Newtonian model, and p_y the yield stress of fluid. We consider a steady state flow. An anonymous referee has suggested considering the value of n = 1. However, in many applications this value is n $\gg$ 1

Under the usual Boussinesq and boundary layer approximations, the equations for mass continuity, momentum and energy, can be written as follows:

$$\frac{\partial(ru)}{\partial x} + \frac{\partial(rv)}{\partial y} = 0 \tag{4}$$

$$u\frac{\partial u}{\partial x} + v\frac{\partial u}{\partial y} = \nu\left(1+\frac{1}{\beta}\right)\frac{\partial^2 u}{\partial y^2} + g\Omega(T-T_\infty)\sin\left(\frac{x}{a}\right) - \frac{\nu}{k}u - \Gamma u^2 \tag{5}$$

$$u\frac{\partial T}{\partial x} + v\frac{\partial T}{\partial y} = \alpha\frac{\partial^2 T}{\partial y^2} \tag{6}$$

where u and v are the velocity components in the x - and y- directions respectively, ν - the kinematic viscosity of the conducting fluid, β - is the non-Newtonian Casson parameter, α - the thermal diffusivity, Ω is the coefficients of thermal expansion,T - the temperature respectively.

The boundary conditions are prescribed at the sphere surface and the edge of the boundary layer regime, respectively as follows:

$$\begin{array}{llll} at & y=0, & u = N_0\left(1+\frac{1}{\beta}\right)\frac{\partial u}{\partial y}, \quad v=-V_w, & T = T_w + K_0\frac{\partial T}{\partial y}; \\ as & y\to\infty, & u\to 0, & T\to T_\infty, \end{array} \tag{7}$$

where N_0 is the velocity slip factor and K_0 is the thermal slip factor. For $N_0 = 0 = K_0$, one can recover the no-slip case.

The stream function ψ is defined by $ru = \partial(r\psi)/\partial y$ and $rv = \partial(r\psi)/\partial x$, and therefore, the continuity equation is automatically satisfied. In order to write the governing equations and the boundary conditions in dimensionless form, the following non-dimensional quantities are introduced.

$$\begin{array}{llll} \xi = \frac{x}{a}, & \eta = \frac{y}{a}\sqrt[4]{Gr}, & f(\xi,\eta) = \frac{\psi}{\nu\xi\sqrt[4]{Gr}}, & \Pr = \frac{\nu}{\alpha}, \\ \theta(\xi,\eta) = \frac{T-T_\infty}{T_w-T_\infty}, & Gr = \frac{g\Omega(T_w-T_\infty)a^3}{\nu^2}, & & \beta = \mu_B\frac{\sqrt{2\pi_c}}{p_y}, \\ \Lambda = \Gamma a, & Da = \frac{K}{a^2}, & & f_w = -\frac{V_w a}{\nu\sqrt[4]{Gr}}, \end{array} \tag{8}$$

where ρ- the density, T_∞- the free stream temperature, V_w - the uniform blowing/suction velocity. In view of Equation (8), Equations (4)-(6) reduce to the following coupled, nonlinear, dimensionless partial differential equations for momentum and energy for the regime

$$\left(1+\frac{1}{\beta}\right)f''' + (1+\xi\cot\xi)\,ff'' - (1+\xi\Lambda)\,f'^2, \\ -\frac{1}{DaGr^{1/2}}f' + \frac{\sin\xi}{\xi}\theta = \xi\left(f'\frac{\partial f'}{\partial\xi} - f''\frac{\partial f}{\partial\xi}\right), \tag{9}$$

$$\frac{\theta''}{\Pr} + (1 + \xi \cot \xi) f\theta' = \xi \left(f' \frac{\partial \theta}{\partial \xi} - \theta' \frac{\partial f}{\partial \xi} \right). \tag{10}$$

The transformed dimensionless boundary conditions are:

$$\begin{aligned} &\text{at} \quad \eta = 0, \qquad f_w = S, \quad f' = \left(1 + \tfrac{1}{\beta}\right) S_f f''(0), \ \theta = 1 + S_T \theta'(0), \\ &\text{As} \quad \eta \to \infty, \quad f' \to 0, \quad \theta \to 0. \end{aligned} \tag{11}$$

In the above equations, the primes denote the differentiation with respect to η, the dimensionless radial coordinate, and ξ is the dimensionless tangential coordinate, $\Pr = \nu/\alpha$ the Prandtl number, $S_f = (N_0/a)Gr^{1/4}$ and $S_T = (K_0/a)Gr^{1/4}$ are the non-dimensional velocity and thermal slip parameters respectively and $f_w = S = -V_w(a/\nu)Gr^{-1/4}$ is the blowing/suction parameter. Here $f_w < 0$ for $V_w > 0$ (the case of blowing), and $f_w > 0$ for $V_w < 0$ (the case of suction). Of course, the special case of a solid sphere surface corresponds to $f_w = 0$.

The engineering design quantities of physical interest include the skin-friction coefficient and Nusselt number, which are given by:

$$\frac{1}{2} C_f Gr^{-3/4} = \left(1 + \frac{1}{\beta}\right) \xi f''(0), \tag{12}$$

$$\frac{Nu}{\sqrt[4]{Gr}} = -\theta'(0). \tag{13}$$

3 Numerical solution

In this study the efficient Keller-Box implicit difference method has been employed to solve the general flow model defined by equations (9)-(10) with boundary conditions (11). Therefore a more detailed exposition is presented here. This method, originally developed for low speed aerodynamic boundary layers by Keller [28], and has been employed in a diverse range of coupled heat transfer problems. These include Ramachandra Prasad et al.[29-30] and Bég et al.[31].

Essentially 4 phases are central to the Keller Box Scheme. These are

a. Reduction of the N^{th} order partial differential equation system to N first order equations

b. Finite Difference Discretization

c. Quasilinearization of Non-Linear Keller Algebraic Equations

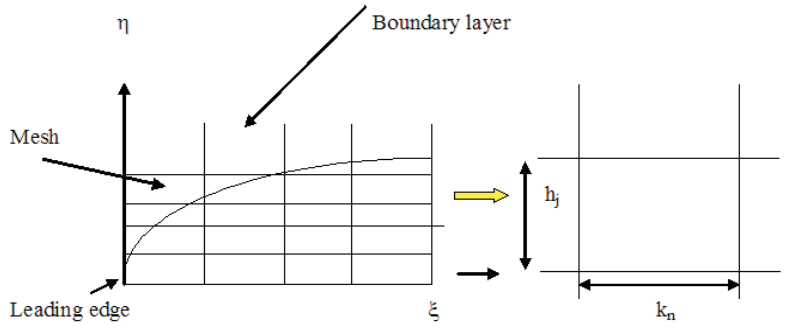

(a) Grid meshing.

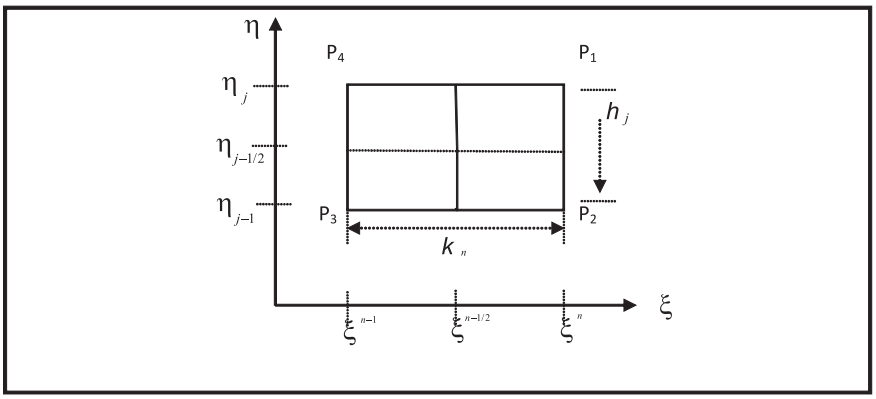

(b) Net "Keller-Box" for difference approximations.

Figure 2: The "Keller Box" computational cell.

d. Block-tridiagonal Elimination of Linear Keller Algebraic Equations

A two-dimensional computational grid is imposed on the $\xi - \eta$ plane as sketched below. The stepping process is defined by:

$$\xi_o = 0; \quad \xi_n = \xi_{n-1} + k_n, \quad n = 1, 2 \ldots, N \tag{14}$$

$$\eta_0 = 0; \quad \eta_j = \eta_{j-1} + h_j, \quad j = 1, 2 \ldots, J \tag{15}$$

where k_n and h_j denote the step distances in the ξ and η directions respectively. Denoting Σ as the value of *any variable* at station (ξ_n, η_j), and the following

central difference approximations are substituted for each reduced variable and their first order derivatives, viz:

$$(\Sigma)_{j1/2}^{n-1/2} = [\Sigma_j^n + \Sigma_{j-1}^n + \Sigma_j^{n-1} + \Sigma_{j-1}^{n-1}]/4, \tag{16}$$

$$(\partial\Sigma/\partial\xi)_{j1/2}^{n-1/2} = [\Sigma_j^n + \Sigma_{j-1}^n - \Sigma_j^{n-1} - \Sigma_{j-1}^{n-1}]/4k_n, \tag{17}$$

$$(\partial\Sigma/\partial\eta)_{j1/2}^{n-1/2} = [\Sigma_j^n + \Sigma_{j-1}^n - \Sigma_j^{n-1} - \Sigma_{j-1}^{n-1}]/4h_j, \tag{18}$$

where k_n = stream wise stepping distance (ξ-mesh spacing) and h_j = span wise stepping distance (η-mesh spacing) defined as follows:

$$\eta_{j-1/2} = [\eta_j + \eta_{j-1}]/2, \tag{19}$$

$$\xi^{n-1/2} = [\xi^n + \xi^{n-1}]/2. \tag{20}$$

Phase a: *Reduction of the N^{th} order partial differential equation system to N first order equations*

Equations (9)-(10) subject to the boundary conditions (11) are first written as a system of first-order equations. For this purpose, we reset Eqns.(9)-(10) as a set of simultaneous equations by introducing the new variables u, v and t:

$$f' = u, \tag{21}$$

$$f" = v, \tag{22}$$

$$\theta' = t, \tag{23}$$

$$\left(1 + \frac{1}{\beta}\right) v' + fv - u^2 + \frac{\sin\xi}{\xi}\theta = \xi\left(u\frac{\partial u}{\partial\xi} - v\frac{\partial f}{\partial\xi}\right), \tag{24}$$

$$\frac{1}{\mathrm{Pr}}t^{'} + ft = \xi\left(u\frac{\partial s}{\partial\xi} - t\frac{\partial f}{\partial\xi}\right), \tag{25}$$

where primes denote differentiation with respect to η.

In terms of the dependent variables, the boundary conditions become:

$$\begin{array}{llll} At & \eta = 0: & u = \left(1 + \frac{1}{\beta}\right) f''(0), \quad f = f_w\,, & s = 1, \\ As & \eta \to \infty: & u \to 0, & s \to 0. \end{array} \tag{26}$$

Phase b: *Finite difference discretization*

The net rectangle considered in the $\xi - \eta$ plane is shown in Fig.2(b), and the net points are denoted by:

$$\xi^0 = 0, \qquad \xi^n = \xi^{n-1} + k_n, \quad n = 1, 2, ..., N, \tag{27}$$

$$\eta_0 = 0, \qquad \eta_j = \eta_{j-1} + h_j, \quad j = 1, 2, ..., J, \qquad \eta_J \equiv \eta_\infty, \tag{28}$$

where k_n is the $\Delta\xi$- spacing and h_j is the $\Delta\eta$- spacing. Here n and j are just sequence numbers that indicate the coordinate location. We approximate the quantities (f, u, v, s, t) at points (ξ^n, η_j) of the net by (f_j^n, u_j^n, v_j^n, s_j^n, t_j^n), which we denote as net functions. We also employ the notion $(\ )_j^n$ for points and quantities midway between net points and for any net function:

$$\xi^{n-1/2} \equiv \frac{1}{2}\left(\xi^n + \xi^{n-1}\right), \qquad \eta_{j-1/2} \equiv \frac{1}{2}\left(\eta_j + \eta_{j-1}\right), \tag{29}$$

$$()_j^{n-1/2} = \frac{1}{2}\left[()_j^n + ()_j^{n-1}\right] \quad and \quad ()_{j-1/2}^n = \frac{1}{2}\left[()_j^n + ()_{j-1}^n\right]. \tag{30}$$

The derivatives in the x - direction are replaced by finite difference approximations. For any net function ( ), generally we have:

$$\frac{\partial\,()}{\partial\xi} = \frac{()^n - ()^{n-1}}{k_n}. \tag{31}$$

We write the difference equations that are to approximate equations (21)-(25) by considering one mesh rectangle as shown in Fig.2(b). We start by writing the finite-difference approximations of the ordinary differential equations (21)-(23) for the midpoint $(\xi^n, \eta_{j-1/2})$ of the process called "centering about $(\xi^n, \eta_{j-1/2})$". This gives: segment P_1 P_2, using centered-difference derivatives.

$$\frac{\left(f_j^n - f_{j-1}^n\right)}{h_j} = \frac{1}{2}\left(u_j^n + u_{j-1}^n\right) = u_{j-1/2}^n, \tag{32}$$

$$\frac{\left(u_j^n - u_{j-1}^n\right)}{h_j} = \frac{1}{2}\left(v_j^n + v_{j-1}^n\right) = v_{j-1/2}^n, \tag{33}$$

$$\frac{\left(s_j^n - s_{j-1}^n\right)}{h_j} = \frac{1}{2}\left(t_j^n + t_{j-1}^n\right) = t_{j-1/2}^n. \tag{34}$$

The finite-difference forms of the partial differential equations (24)-(25) are approximated by centering about the midpoint $\left(\xi^{n-1/2}, \eta_{j-1/2}\right)$ of the rectangle $P_1P_2P_3P_4$. This can be done in two steps. In the first step, we center equations (24)-(25) about the point $\left(\xi^{n-1/2}, \eta\right)$ without specifying y. The differenced

version of equations (24)-(25) at $\xi^{n-1/2}$ then take the form:

$$\left(1+\frac{1}{\beta}\right)\left(v'\right)^n+\left(1+\alpha+\xi Cot\xi\right)\left(fv\right)^n-\left(1+\alpha+\xi\Lambda\right)\left(u^2\right)^n$$
$$+\alpha v^{n-1}f^n-\alpha f^{n-1}v^n+Bs^n=\left[-\left(1+\frac{1}{\beta}\right)\left(v'\right)\right. \tag{35}$$
$$\left.-\left(1-\alpha+\xi Cot\xi\right)\left(fv\right)+\left(1-\alpha+\xi\Lambda\right)\left(u^2\right)-B\left(s\right)\right]^{n-1},$$

$$\frac{1}{\mathrm{Pr}}\left(t'\right)^n+\left(1+\alpha+\xi Cot\xi\right)\left(ft\right)^n-\alpha\left(us\right)^n+\alpha s^{n-1}u^n$$
$$-\alpha u^{n-1}s^n-\alpha f^{n-1}t^n+\alpha t^{n-1}f^n \tag{36}$$
$$=\left[-\frac{1}{\mathrm{Pr}}\left(t'\right)+\left(\alpha-1-\xi Cot\xi\right)\left(ft\right)-\alpha\left(us\right)\right]^{n-1}.$$

Here we have used the abbreviations

$$\alpha=\frac{\xi^{n-1/2}}{k_n}, \tag{37}$$
$$B=\frac{\sin\left(\xi^{n-1/2}\right)}{\xi^{n-1/2}} \tag{38}$$

and where the notation $[\quad]^{n-1}$ corresponds to quantities in the square bracket evaluated at $\xi=\xi^{n-1}$.

Next, we center equations (35)-(36) about the point $\left(\xi^{n-1/2},\,\eta_{j-1/2}\right)$ by using equations (29) & (30) yielding:

$$\left(1+\frac{1}{\beta}\right)\left(\frac{v_j^n-v_{j-1}^n}{h_j}\right)+\left(1+\alpha+\xi Cot\xi\right)\left(f_{j-1/2}^n v_{j-1/2}^n\right)$$
$$-\left(1+\alpha+\xi\Lambda\right)\left(u_{j-1/2}^n\right)^2+\alpha v_{j-1/2}^{n-1}f_{j-1/2}^n-\alpha f_{j-1/2}^{n-1}v_{j-1/2}^n$$
$$+B\left(s_{j-1/2}^n\right)-\left(\frac{1}{DaGr^{1/2}}\right)\left(u_{j-1/2}^n\right) \tag{39}$$
$$=-\left[\left(1+\frac{1}{\beta}\right)\left(\frac{v_j^{n-1}-v_{j-1}^{n-1}}{h_j}\right)+\left(1-\alpha\right)\left(f_{j-1/2}^{n-1}v_{j-1/2}^{n-1}\right)\right.$$
$$\left.+\left(\alpha-1\right)\left(u_{j-1/2}^{n-1}\right)^2+B\left(s_{j-1/2}^{n-1}\right)\right]$$

$$\frac{1}{\Pr}\left(\frac{t_j^n - t_{j-1}^n}{h_j}\right) + (1+\alpha+\xi Cot\xi)\left(f_{j-1/2}^n t_{j-1/2}^n\right)$$
$$-\alpha\left(u_{j-1/2}^n s_{j-1/2}^n\right) + \alpha s_{j-1/2}^{n-1} u_{j-1/2}^n - \alpha u_{j-1/2}^{n-1} s_{j-1/2}^n$$
$$-\alpha f_{j-1/2}^{n-1} t_{j-1/2}^n + \alpha t_{j-1/2}^{n-1} f_{j-1/2}^n \tag{40}$$
$$= -\left[\frac{1}{\Pr}\left(\frac{t_j^{n-1} - t_{j-1}^{n-1}}{h_j}\right) + \alpha\left(u_{j-1/2}^{n-1} s_{j-1/2}^{n-1}\right)\right.$$
$$\left.+(1-\alpha+\xi Cot\xi)\left(f_{j-1/2}^{n-1} t_{j-1/2}^{n-1}\right)\right]$$

Equations (32)-(34) and (39)-(40) are imposed for $j = 1, 2 \ldots, J$ at given n, and the transformed boundary layer thickness, η_J is to be sufficiently large so that it is beyond the edge of the boundary layer. At $\xi = \xi^n$, the boundary conditions (26) become

$$f_0^n = u_0^n = 0, \quad \theta_0^n = 1, \quad u_j^n = 0, \quad \theta_0^n = 0 \tag{41}$$

Phase c: *Quasilinearization of Non-Linear Keller Algebraic Equations*

If we assume f_j^{n-1}, u_j^{n-1}, v_j^{n-1}, s_j^{n-1}, t_j^{n-1} to be known for $0 \leq j \leq J$, Equations (32)-(36) are a system of $5J+5$ equations for the solution of $5J+5$ unknowns f_j^n, u_j^n, v_j^n, s_j^n, t_j^n, $j = 0, 1, 2 \ldots, J$. This non-linear system of algebraic equations is linearized by means of Newton's method as explained by Ramachandra Prasad et.al (2011).

Newton's Method is then employed to quasilinearize the equations (39)-(40). If we assume f_j^{n-1}, u_j^{n-1}, v_j^{n-1}, s_j^{n-1}, t_j^{n-1} to be known for $0 \leq j \leq J$, then Equations (32-34) and (39-40) are a system of equations for the solution of the unknowns $(f_j^n, u_j^n, v_j^n, s_j^n, t_j^n)$, $j = 0, 1, 2, \ldots, J$.

For simplicity of notation we shall write the unknowns at $\xi = \xi^n$ as:

$$(f_j^n, u_j^n, v_j^n, s_j^n, t_j^n) \equiv (f_j, u_j, v_j, s_j, t_j). \tag{42}$$

Then the system of equations (32)-(34) and (39)-(40) can be written as (after multiplying with h_j)

$$f_j - f_{j-1} - \frac{h_j}{2}(u_j + u_{j-1}) = 0, \tag{43}$$

$$u_j - u_{j-1} - \frac{h_j}{2}(v_j + v_{j-1}) = 0, \tag{44}$$

$$s_j - s_{j-1} - \frac{h_j}{2}(t_j + t_{j-1}) = 0, \tag{45}$$

$$\begin{aligned}
&\left(1+\tfrac{1}{\beta}\right)(v_j-v_{j-1})+\tfrac{(1+\alpha+\xi Cot\xi)h_j}{4}\left[(f_j+f_{j-1})(v_j+v_{j-1})\right]\\
&-\tfrac{h_j}{4}(1+\alpha+\xi\Lambda)(u_j+u_{j-1})^2+\tfrac{\alpha h_j}{2}v^{n-1}_{j-1/2}(f_j+f_{j-1})\\
&-\tfrac{\alpha h_j}{2}f^{n-1}_{j-1/2}(v_j+v_{j-1})+\tfrac{Bh_j}{2}\left[s_j+s_{j-1}\right]\\
&-\tfrac{h_j}{2DaGr^{1/2}}\left[u_j+u_{j-1}\right]=[R_1]^{n-1}_{j-1/2},
\end{aligned}\tag{46}$$

$$\begin{aligned}
&\tfrac{1}{\Pr}(t_j-t_{j-1})+\tfrac{(1+\alpha+\xi Cot\xi)h_j}{4}\left[(f_j+f_{j-1})(t_j+t_{j-1})\right]\\
&-\tfrac{\alpha h_j}{4}\left[(u_j+u_{j-1})(s_j+s_{j-1})\right]+\tfrac{\alpha h_j}{2}s^{n-1}_{j-1/2}(u_j+u_{j-1})\\
&-\tfrac{\alpha h_j}{2}u^{n-1}_{j-1/2}(s_j+s_{j-1})-\tfrac{\alpha h_j}{2}f^{n-1}_{j-1/2}(t_j+t_{j-1})\\
&+\tfrac{\alpha h_j}{2}t^{n-1}_{j-1/2}(f_j+f_{j-1})=[R_2]^{n-1}_{j-1/2},
\end{aligned}\tag{47}$$

where

$$\begin{aligned}
[R_1]^{n-1}_{j-1/2}=-h_j\Bigg[&\left(1+\frac{1}{\beta}\right)\left(\frac{v_j-v_{j-1}}{h_j}\right)\\
&+(1-\alpha+\xi\cot\xi)\left(f^v_{j-1/2j-1/2}\right)\\
&(1-\alpha+\xi\Lambda)\left(u_{j-1/2}\right)^2\\
&-\frac{1}{DaGr^{1/2}}u_{j-1/2}+B\left(s_{j-1/2}\right)\Bigg],
\end{aligned}\tag{48}$$

$$\begin{aligned}
[R_2]^{n-1}_{j-1/2} \;=\; &-h_j\Bigg[\frac{1}{\Pr}\left(\frac{t_j-t_{j-1}}{h_j}\right)+\alpha\left(u^s_{j-1/2j-1/2}\right)\\
&+(1-\alpha+\xi\cot\xi)\left(f^t_{j-1/2j-1/2}\right).\Bigg]
\end{aligned}\tag{49}$$

Here $[R_1]^{n-1}_{j-1/2}$ and $[R_2]^{n-1}_{j-1/2}$ involve only known quantities if we assume that solution is known on $\xi=\xi^{n-1}$.

To linearize the nonlinear system of equations (43-47) using Newton's method, we introduce the following iterates:

$$f_j^{(i+1)} = f_j^{(i)} + \delta f_j^{(i)}, \quad u_j^{(i+1)} = u_j^{(i)} + \delta u_j^{(i)}, \quad v_j^{(i+1)} = v_j^{(i)} + \delta v_j^{(i)},$$
$$s_j^{(i+1)} = s_j^{(i)} + \delta s_j^{(i)}, \quad t_j^{(i+1)} = t_j^{(i)} + \delta t_j^{(i)}. \tag{50}$$

Then we substitute these expressions into Equations (43)-(47) except for the term ξ^{n-1}, and this yields:

$$\left(f_j^{(i)} + \delta f_j^{(i)}\right) - \left(f_{j-1}^{(i)} + \delta f_{j-1}^{(i)}\right) - \frac{h_j}{2}\left(u_j^{(i)} + \delta u_j^{(i)} + u_{j-1}^{(i)} + \delta u_{j-1}^{(i)}\right) = 0, \tag{51}$$

$$\left(u_j^{(i)} + \delta u_j^{(i)}\right) - \left(u_{j-1}^{(i)} + \delta u_{j-1}^{(i)}\right) - \frac{h_j}{2}\left(v_j^{(i)} + \delta v_j^{(i)} + v_{j-1}^{(i)} + \delta v_{j-1}^{(i)}\right) = 0, \tag{52}$$

$$\left(s_j^{(i)} + \delta s_j^{(i)}\right) - \left(s_{j-1}^{(i)} + \delta s_{j-1}^{(i)}\right) - \frac{h_j}{2}\left(t_j^{(i)} + \delta t_j^{(i)} + t_{j-1}^{(i)} + \delta t_{j-1}^{(i)}\right) = 0, \tag{53}$$

$$\begin{aligned}[R_1]_{j-1/2}^{n-1} = {} & \left(1 + \frac{1}{\beta}\right)\left[\left(v_j^{(i)} + \delta v_j^{(i)}\right) - \left(v_{j-1}^{(i)} + \delta v_{j-1}^{(i)}\right)\right] \\ & - \frac{h_j}{4}\left(1 + \alpha + \xi\Lambda\right)\left(u_j^{(i)} + \delta u_j^{(i)} + u_{j-1}^{(i)} + \delta u_{j-1}^{(i)}\right)^2 \\ & + \left(1 + \alpha + \xi Cot\xi\right)\left(h_j/4\right)\left[\left(f_j^{(i)} + \delta f_j^{(i)} + f_{j-1}^{(i)}\right.\right. \\ & \left.\left. + \ \delta f_{j-1}^{(i)}\right)\left(v_j^{(i)} + \delta v_j^{(i)} + v_{j-1}^{(i)} + \delta v_{j-1}^{(i)}\right)\right] \end{aligned} \tag{54}$$

$$
\begin{aligned}
&+\frac{\alpha h_j}{2}v_{j-1/2}^{n-1}\left(f_j^{(i)}+\delta f_j^{(i)}+f_{j-1}^{(i)}+\delta f_{j-1}^{(i)}\right)\\
&-\frac{\alpha h_j}{2}f_{j-1/2}^{n-1}\left(v_j^{(i)}+\delta v_j^{(i)}+v_{j-1}^{(i)}+\delta v_{j-1}^{(i)}\right)\\
&-\frac{h_j}{2DaGr^{1/2}}\left(u_j^{(i)}+\delta u_j^{(i)}+u_{j-1}^{(i)}+\delta u_{j-1}^{(i)}\right)\\
&+\frac{Bh_j}{2}\left(s_j^{(i)}+\delta s_j^{(i)}+s_{j-1}^{(i)}+\delta s_{j-1}^{(i)}\right),
\end{aligned}
\qquad (54-contd)
$$

$$
\begin{aligned}
[R_2]_{j-1/2}^{n-1} &= \frac{1}{\mathrm{Pr}}\left[\left(t_j^{(i)}+\delta t_j^{(i)}\right)-\left(t_{j-1}^{(i)}+\delta t_{j-1}^{(i)}\right)\right]\\
&+(1+\alpha+\xi Cot\xi)\,(h_j/4)\left[\left(f_j^{(i)}+\delta f_j^{(i)}+f_{j-1}^{(i)}\right.\right.\\
&\left.\left.+\delta f_{j-1}^{(i)}\right)\left(t_j^{(i)}+\delta t_j^{(i)}+t_{j-1}^{(i)}+\delta t_{j-1}^{(i)}\right)\right]\\
&-\frac{\alpha h_j}{4}\left[\left(u_j^{(i)}+\delta u_j^{(i)}+u_{j-1}^{(i)}+\delta u_{j-1}^{(i)}\right)\left(s_j^{(i)}\right.\right.\\
&\left.\left.+\ \delta s_j^{(i)}+s_{j-1}^{(i)}+\delta s_{j-1}^{(i)}\right)\right]\\
&+\frac{\alpha h_j}{2}s_{j-1/2}^{n-1}\left(u_j^{(i)}+\delta u_j^{(i)}+u_{j-1}^{(i)}+\delta u_{j-1}^{(i)}\right)\\
&-\frac{\alpha h_j}{2}u_{j-1/2}^{n-1}\left(s_j^{(i)}+\delta s_j^{(i)}+s_{j-1}^{(i)}+\delta s_{j-1}^{(i)}\right)\\
&-\frac{\alpha h_j}{2}f_{j-1/2}^{n-1}\left(t_j^{(i)}+\delta t_j^{(i)}+t_{j-1}^{(i)}+\delta t_{j-1}^{(i)}\right)\\
&+\frac{\alpha h_j}{2}t_{j-1/2}^{n-1}\left(f_j^{(i)}+\delta f_j^{(i)}+f_{j-1}^{(i)}+\delta f_{j-1}^{(i)}\right),
\end{aligned}
\qquad (55)
$$

Next we drop the terms that are quadratic in the following $\left(\delta f_j^{(i)},\ \delta u_j^{(i)}\ ,\ \delta v_j^{(i)},\ \delta s_j^{(i)},\ \delta t_j^{(i)}\right)$. We also drop the superscript i for simplicity. After some algebraic manipulations, the following linear tridiagonal system of equations is obtained:

$$
\delta f_j-\delta f_{j-1}-\frac{h_j}{2}\left(\delta u_j+\delta u_{j-1}\right)=(r_1)_{j-1/2}, \qquad (56)
$$

$$
\delta u_j-\delta u_{j-1}-\frac{h_j}{2}\left(\delta v_j+\delta v_{j-1}\right)=(r_2)_{j-1/2}, \qquad (57)
$$

$$\delta s_j - \delta s_{j-1} - \frac{h_j}{2}\left(\delta t_j + \delta t_{j-1}\right) = (r_3)_{j-1/2}, \tag{58}$$

$$\begin{aligned}(r_4)_{j-1/2} = (a_1)_j \delta v_j + (a_2)_j \delta v_{j-1} + (a_3)_j \delta f_j + (a_4)_j \delta f_{j-1} \\ + (a_5)_j \delta u_j + (a_6)_j \delta u_{j-1} + (a_7)_j \delta s_j + (a_8)_j \delta s_{j-1},\end{aligned} \tag{59}$$

$$\begin{aligned}(r_5)_{j-1/2} = (b_1)_j \delta t_j + (b_2)_j \delta t_{j-1} + (b_3)_j \delta f_j + (b_4)_j \delta f_{j-1} \\ + (b_5)_j \delta u_j + (b_6)_j \delta u_{j-1} + (b_7)_j \delta s_j + (b_8)_j \delta s_{j-1},\end{aligned} \tag{60}$$

where

$$\begin{aligned}(a_1)_j &= \left(1 + \frac{1}{\beta}\right) + h_j \left[\frac{(1+\alpha+\xi Cot\xi)}{2} f_{j-1/2} - \frac{\alpha}{2} f^{n-1}_{j-1/2}\right] \\ (a_2)_j &= (a_2)_j - 2\left(1 + \frac{1}{\beta}\right), \\ (a_3)_j &= h_j \left[\frac{(1+\alpha+\xi Cot\xi)}{2} v_{j-1/2} + \frac{\alpha}{2} v^{n-1}_{j-1/2}\right] \\ (a_4)_j &= (a_3)_j, \\ (a_5)_j &= -\left(1+\alpha+\xi\Lambda\right) h_j u_{j-1/2} - \frac{h_j}{2DaGr^{1/2}}, \\ (a_6)_j &= (a_5)_j, \qquad (a_7)_j = \frac{B}{2} h_j, \qquad (a_8)_j = (a_7)_j\end{aligned} \tag{61}$$

$$\begin{aligned}(b_1)_j &= \frac{1}{\mathrm{Pr}} + h_j \left[\frac{(1+\alpha+\xi Cot\xi)}{2} f_{j-1/2} - \frac{\alpha}{2} f^{n-1}_{j-1/2}\right], \\ (b_2)_j &= (b_1)_j - \frac{2}{\mathrm{Pr}} \\ (b_3)_j &= h_j \left[\frac{(1+\alpha+\xi Cot\xi)}{2} t_{j-1/2} + \frac{\alpha}{2} t^{n-1}_{j-1/2}\right], \quad (b_4)_j = (b_3)_j, \\ (b_5)_j &= h_j \left[-\frac{\alpha}{2} s_{j-1/2} + \frac{\alpha}{2} s^{n-1}_{j-1/2}\right], \quad (b_6)_j = (b_5)_j, \\ (b_7)_j &= h_j \left[-\frac{\alpha}{2} u_{j-1/2} - \frac{\alpha}{2} u^{n-1}_{j-1/2}\right], \quad (b_8)_j = (b_7)_j\end{aligned} \tag{62}$$

$$(r_1)_{j-1/2} = f_{j-1} - f_j + h_j u_{j-1/2}, \quad (r_2)_{j-1/2} = u_{j-1} - u_j + h_j v_{j-1/2},$$
$$(r_3)_{j-1/2} = s_{j-1} - s_j + h_j t_{j-1/2},$$
$$(r_4)_{j-1/2} = \left(1 + \frac{1}{\beta}\right)(v_{j-1} - v_j) - (1 + \alpha + \xi Cot\xi)\, h_j f_{j-1/2} v_{j-1/2} \tag{63}$$
$$+ h_j\,(1 + \alpha + \xi\Lambda)\, u^2_{j-1/2} - \alpha h_j v^{n-1}_{j-1/2} f_{j-1/2} + \alpha h_j f^{n-1}_{j-1/2} v_{j-1/2}$$
$$- B h_j s_{j-1/2} + \frac{h_j}{DaGr^{1/2}}\,(R_1)^{n-1}_{j-1/2}\,,$$

To complete the system (56)-(60), we recall the boundary conditions (41), which can be satisfied exactly with no iteration. Therefore to maintain these correct values in all the iterates, we take:

$$\delta f_0^{=} 0, \quad \delta u_0^{=} 0, \quad \delta s_0^{=} 0, \quad \delta u_J^{=} 0, \quad \delta s_J^{=} 0 \tag{64}$$

Phase d: *Block-tridiagonal Elimination of Linear Keller Algebraic Equations*

The linear system (56)-(60) can now be solved by the block-elimination method. The linearized difference equations of the system (56)-(60) have a block-tridiagonal structure. Commonly, the block-tridiagonal structure consists of variables or constants, but here, an interesting feature can be observed that is, for the Keller-box method, it consists of block matrices. Before we can proceed further with the block-elimination method, we will show how to get the elements of the block matrices from the linear system (56)-(60). We consider three cases, namely when $j = 1, J-1$ and J. When $j = 1$, the linear system (56)-(60) becomes:

$$\delta f_1 - \delta f_0 - \frac{h_1}{2}\,(\delta u_1 + \delta u_0) = (r_1)_{1-1/2}, \tag{65}$$

$$\delta u_1 - \delta u_0 - \frac{h_j}{2}\,(\delta v_1 + \delta v_0) = (r_2)_{1-1/2}, \tag{66}$$

$$\delta s_1 - \delta s_0 - \frac{h_j}{2}\,(\delta t_1 + \delta t_0) = (r_3)_{1-1/2}, \tag{67}$$

$$(r_4)_{1-1/2} = (a_1)_1 \delta v_1 + (a_2)_1 \delta v_0 + (a_3)_1 \delta f_1 + (a_4)_1 \delta f_0 \tag{68}$$
$$+ (a_5)_1 \delta u_1 + (a_6)_1 \delta u_0 + (a_7)_1 \delta s_1 + (a_8)_1 \delta s_0,$$

$$(r_6)_{1-1/2} = (b_1)_1\delta t_1 + (b_2)_1\delta t_0 + (b_3)_1\delta f_1 + (b_4)_1\delta f_0 + (b_5)_1\delta u_1 + (b_6)_1\delta u_0 + (b_7)_1\delta s_1 + (b_8)_1\delta s_0, \tag{69}$$

Designating $d_1 = -\frac{1}{2}h_1$, *and* $\delta f_0 = 0, \quad \delta u_0 = 0, \quad \delta s_0 = 0$ the corresponding matrix form assumes:

$$\begin{bmatrix} 0 & 0 & 1 & 0 & 0 \\ d_1 & 0 & 0 & d_1 & 0 \\ 0 & d_1 & 0 & 0 & d_1 \\ a_2 & 0 & a_3 & a_1 & 0 \\ 0 & b_2 & b_3 & 0 & b_1 \end{bmatrix} \begin{bmatrix} \delta v_0 \\ \delta t_0 \\ \delta f_1 \\ \delta v_1 \\ \delta t_1 \end{bmatrix} + \begin{bmatrix} d_1 & 0 & 0 & 0 & 0 \\ 1 & 0 & 0 & 0 & 0 \\ 0 & 1 & 0 & 0 & 0 \\ a_5 & a_7 & 0 & 0 & 0 \\ b_5 & b_7 & 0 & 0 & 0 \end{bmatrix} \begin{bmatrix} \delta u_1 \\ \delta s_1 \\ \delta f_2 \\ \delta v_2 \\ \delta t_2 \end{bmatrix} = \begin{bmatrix} (r_1)_{1-(1/2)} \\ (r_2)_{1-(1/2)} \\ (r_3)_{1-(1/2)} \\ (r_4)_{1-(1/2)} \\ (r_5)_{1-(1/2)} \end{bmatrix} \tag{70}$$

For $j = 1$, we have $[A_1]\,[\delta_1] + [C_1]\,[\delta_2] = [r_1]$.

Similar procedures are followed at the different stations. Effectively the five linearized finite difference equations have the matrix-vector form:

$$\mathbf{\Lambda}\delta_j = \zeta_j \tag{71}$$

where Λ = Keller coefficient matrix of order 5 x 5, δ_j = fifth order vector for error (perturbation) quantities and ζ_j= fifth order vector for Keller residuals. This system is then recast as an expanded matrix-vector system, viz:

$$\varsigma_{\,j}\delta_j - \omega_j\delta_j = \zeta_j \tag{72}$$

Where now $\varsigma_{\,j}$= coefficient matrix of order 5 x 5, ω_j = coefficient matrix of order 5 x 5 and ζ_j= fifth order vector of errors (iterates) at previous station on grid. Finally the complete linearized system is formulated as a *block matrix system* where each element in the coefficient matrix is a matrix itself.

Then, this system is solved using the efficient Keller-box method as developed by Cebeci and Bradshaw [32]. The numerical results are affected by the number of mesh points in both directions. Accurate results are produced by performing a mesh sensitivity analysis. After some trials in the η-direction a larger number of mesh points are selected whereas in the ξ direction significantly less mesh points are utilized. η_{max} has been set at 16 and this defines

an adequately large value at which the prescribed boundary conditions are satisfied. ξ_{max} is set at 3.0 for this flow domain. These calculations are repeated until some convergence criterion is satisfied. *Mesh independence* is therefore achieved in the present computations. The computer program of the algorithm is executed in *MATLAB* running on a PC. The method demonstrates excellent stability, convergence and consistency, as elaborated by Keller [33].

4 Results and discussions

In order to verify the accuracy of our present method, we have compared our results with those of Merkin [35] and Yih [34]. Table 1 shows these comparisons. Comprehensive solutions have been obtained and are presented in Figs.

Table 1: The Local Heat Transfer Coefficient (Nu) for various values of $\xi$with$\beta \to \infty, f_w = 0, N_0 = 0, K_0 = 0$.

ξ	$-\theta'(\xi, 0)$		
	Merkin[35]	Yin[34]	Present results
0.0	0.4212	0.4214	0.4211
0.2	0.4204	0.4207	0.4205
0.4	0.4182	0.4184	0.4186
0.6	0.4145	0.4147	0.4148
0.8	0.4093	0.4096	0.4094
1.0	0.4025	0.4030	0.4033
1.2	0.3942	0.3950	0.3949
1.4	0.3843	0.3854	0.3855
1.6	0.3727	0.3740	0.3738
1.8	0.3594	0.3608	0.3600
2.0	0.3443	0.3457	0.3454
2.2	0.3270	0.3283	0.3278
2.4	0.3073	0.3086	0.3081
2.6	0.2847	0.2860	0.2855
2.8	0.2581	0.2595	0.2587
3.0	0.2252	0.2267	0.2265
π	0.1963	0.1963	0.1960

3-24. The numerical problem comprises two independent variables (ξ,η), two dependent fluid dynamic variables (f, θ) and eight thermophysical and body force control parametersPr, $S_f, S_T, \beta, f_w, \xi, Da$ and Λ. In the present computa-

tions, the following default parameters are prescribed (unless otherwise stated): $Pr = 0.71, S_f = 0.5$, $S_T = 1.0$, $\beta = 1.0, Da = 0.1$, $\Lambda = 0.1$, $f_w = 0.5$, $\xi = 1.0$. In addition we also consider the effect of stream wise (transverse) coordinate location on flow dynamics.

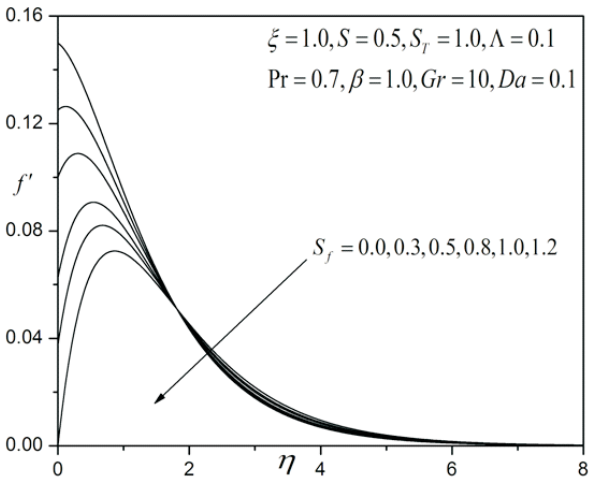

Figure 3: Influence of S_f on velocity profiles

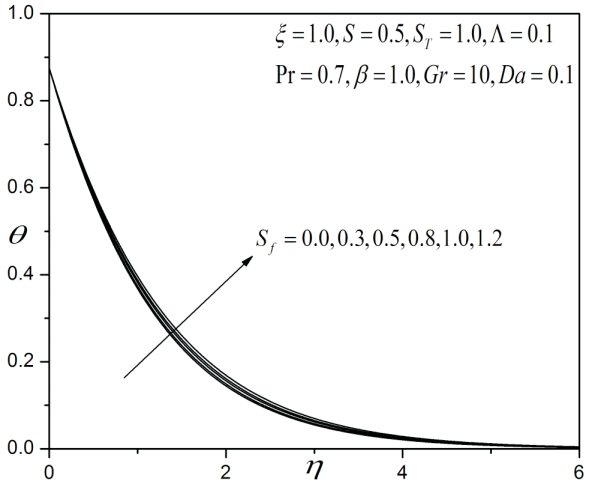

Figure 4: Influence of S_f on temperature profiles

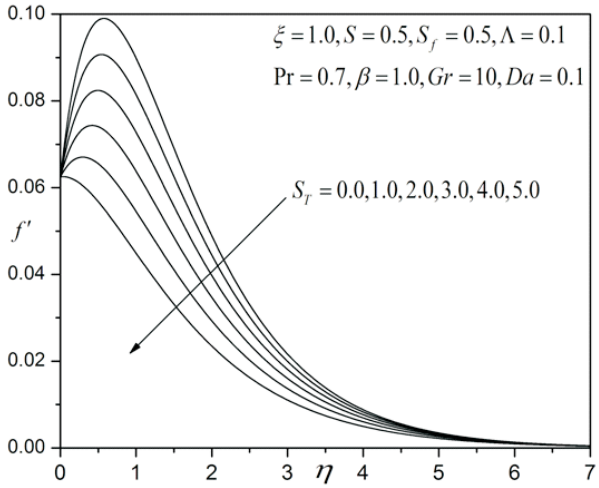

Figure 5: Influence of S_T on velocity profiles

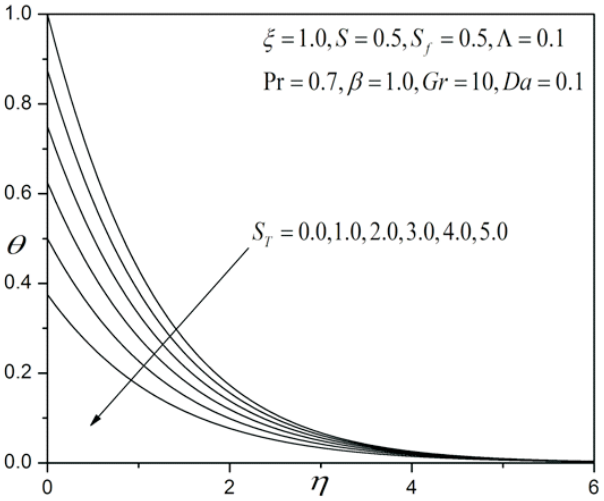

Figure 6: Influence of S_T on temperature profiles

The value of the parameter ξ is extremely important. For $\xi \sim 0$, the location is in the vicinity of the lower stagnation point on the sphere. The governing dimensionless equations (8) to (9) in this case reduce to the following ordinary

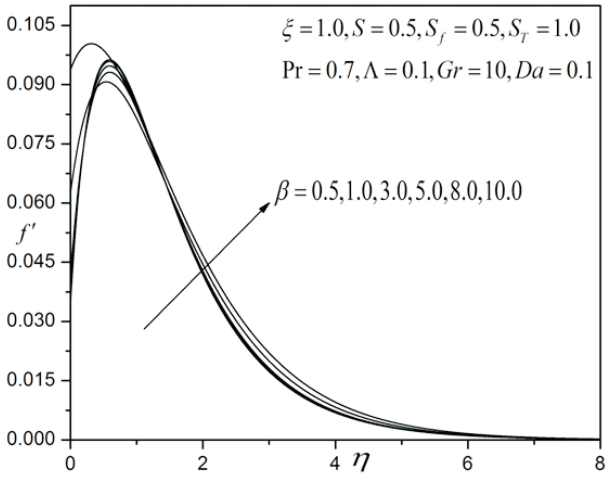

Figure 7: Influence of β on velocity profiles

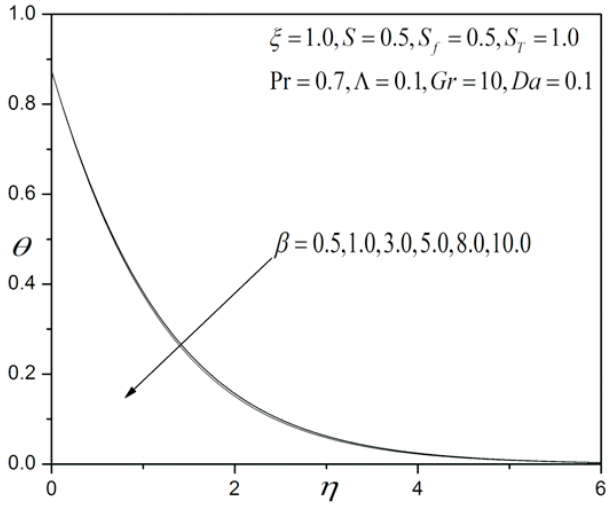

Figure 8: Influence of β on temperature profiles

differential equations:

$$\left(1 + \frac{1}{\beta}\right) f''' + 2ff'' - f'^2 - \frac{1}{DaGr^{1/2}} f' + \theta = 0, \tag{73}$$

$$\frac{\theta''}{\Pr} + 2f\theta' = 0, \tag{74}$$

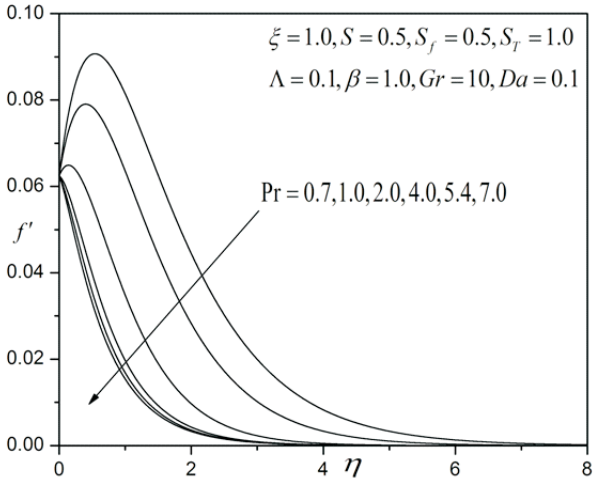

Figure 9: Influence of Pr on velocity profiles

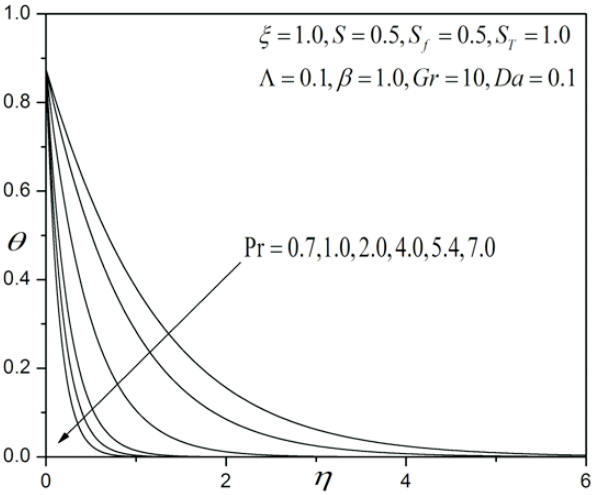

Figure 10: Influence of Pr on temperature profiles

since $\frac{\sin\varsigma}{\varsigma} \rightarrow \quad 0/0$ i.e. 1, so that $\frac{\sin\varsigma}{\varsigma}\ \theta \rightarrow \theta$. Another special case arises at $\xi \sim \pi$, which physically corresponds to the *upper stagnation point* on the sphere surface (diametrically opposite to the lower stagnation point). We note that since the Grashof free convection parameter, Gr, is absorbed into the definitions for radial coordinate (η) and dimensionless stream function (f), it is not considered explicitly in the graphs. In Figs.3-4, the influence of

velocity slip parameter on velocity and temperature distributions is illustrated. Dimensionless velocity component (fig.3) at the wall is strongly reduced with an increase in slip parameter, S_f. There will be a corresponding decrease in the momentum (velocity) boundary layer thickness. The influence of S_f is evidently more pronounced closer to the sphere surface ($\eta = 0$). Further from the surface, there is a transition in *velocity slip effect*, and the flow is found to be accelerated markedly. Smooth decays of the velocity profiles are observed into the free stream demonstrating excellent convergence of the numerical solution. Furthermore the acceleration near the wall with increasing velocity slip effect has been computed by Crane and McVeigh [36] using asymptotic methods, as has the retardation in flow further from the wall. The switch in velocity slip effect on velocity evolution has also been observed for the case of a power-law rheological fluid by Ojadi *et al.* [37]. Fig.4 indicates that an increase in velocity slip parameter significantly enhances temperature in the flow field and thereby increases thermal boundary layer thickness enhances. Temperature profiles consistently decay monotonically from a maximum at the sphere surface to the free stream. All profiles converge at large value of radial coordinate, again showing that convergence has been achieved in the numerical computations. A similar pattern of thermal response to that computed in fig 4. for a wide range of velocity slip parameters has been noted by Aziz [38] who has indicated also that temperature is enhanced since increasing velocity slip parameter decreases shear stresses and this permits a more effective transfer of heat from the wall to the fluid regime.

In Figs.5-6, the variation of velocity and temperature with the transverse coordinate (η), with increasing thermal slip parameter S_T is depicted. The response of velocity is much more consistent than for the case of changing velocity slip parameter (fig.3) it is strongly decreased for all locations in the radial direction. The peak velocity accompanies the case of no thermal slip ($S_T = 0$). The maximum deceleration corresponds to the case of strongest thermal slip ($S_T = 5$). Temperatures (fig.6) are also strongly depressed with increasing thermal slip. The maximum effect is observed at the wall. Further into the free stream, all temperature profiles converge smoothly to the vanishing value. The numerical computations correlate well with the results of Larrode *et al.* [39] who also found that temperature is strongly lowered with increasing thermal slip and that this is attributable to the decrease in heat transfer from the wall to the fluid regime, although they considered only a Newtonian fluid.

In Figs.7-8, depict the influence Casson fluid parameter, β on velocity and temperature profiles. This parameter features in the shear term in the momentum boundary layer equation (5), and also in the velocity boundary condition

(7). For Newtonian flow, yield stress p_y is zero and $\beta = \mu_B\sqrt{\pi_c}/p_y \rightarrow \infty$ i.e. the appropriate term in eqn. (7) reduces from $(1 + 1/\beta)f''' \rightarrow 1$. Similarly the velocity boundary condition in (11) reduces from $(1 + 1/\beta)\ S_f f''(0) \rightarrow S_f f''(0)$. An increase in β implies a decrease therefore in yield stress of the Casson fluid. This effectively facilitates flow of the fluid i.e. accelerates the boundary layer flow close to the sphere surface, as demonstrated by fig. 7. Since the Casson parameter is also present in the wall boundary condition, the acceleration effect is only confined to the region close to the sphere surface. Further from this zone, the velocity slip factor, S_f will exert a progressively reduced effect and an increase in Casson parameter,β, will manifest with a deceleration in the flow. Overall however the dominant influence of β, is near the wall and is found to be assistive to momentum development (with larger β values the fluid is closer in behaviour to a *Newtonian* fluid and further departs from *plastic* flow) Only a very small decrease in temperature is observed with a large enhancement in Casson fluid parameter, as shown in fig. 8. The Casson parameter does not arise in the thermal boundary layer equation (10), nor does it feature in the thermal boundary conditions. The influence on temperature field is therefore experienced indirectly via coupling of the thermal eqn. (10) with the momentum eqn. (9). Similar behaviour to the computations shown in Figs. 7 and 8, has been observed by Attia and Sayed-Ahmed [40] who also observed acceleration in Casson fluid flow near a curved surface, and additionally by Mustafa *et al.* [41] who also observed an elevation in velocities near the wall and a slight reduction in temperatures throughout the boundary layer regime.

Figs.9-10, present the effect of Prandtl number (Pr) on the velocity and temperature profiles along the radial direction, normal to the sphere surface. Prandtl number embodies the ratio of *viscous diffusion* to *thermal diffusion* in the boundary layer regime. It also expresses the ratio of the *product of specific heat capacity and dynamic viscosity*, to the *fluid thermal conductivity*. When Pr is high, viscous diffusion rate exceeds thermal diffusion rate. An increase in Pr from 0.7 through 1.0, 2.0, 4.0, 5.4 to 7.0, is found to significantly depress velocities (**Fig.9**) and this trend is sustained throughout the regime i.e. for all values of the radial coordinate,η . For Pr ¡1, thermal diffusivity exceeds momentum diffusivity i.e. heat will diffuse faster than momentum. Therefore for lower Pr fluids (e.g. $Pr = 0.01$ *which physically correspond to liquid metals*), the flow will be accelerates whereas for greater Pr fluids (e.g. $Pr = 1$) it will be *strongly decelerated*, as observed in fig. For $Pr = 1.0$, both the viscous and energy diffusion rates will be the same as will the thermal and velocity boundary layer thicknesses. This case can be representative of food stuffs e.g. low-density polymorphic forms of chocolate suspensions, as noted by Steffe [42] and Debaste

et al. [43]. Temperature is found to be strongly reduced with increasing Prandtl number. For the case of $Pr = 0.7$, the decay is almost exactly *linear*. For larger Pr values, the decay is found to be *increasingly monotonic*. Therefore for lower thermal conductivity fluids (as typified by liquid chocolate and other foodstuffs), lower temperatures are observed throughout the boundary layer regime.

Figs.11-12, illustrate the influence of wall transpiration on the velocity and temperature functions with radial distance, η. With an increase in suction ($f_w > 0$) the velocity is clearly decreased i.e. the flow is decelerated. Increasing suction causes the boundary layer to adhere closer to the flow and destroys momentum transfer; it is therefore an excellent control mechanism for stabilizing the external boundary layer flow on the sphere. Conversely with increased blowing i.e. injection of fluid via the sphere surface in to the porous medium regime, ($f_w < 0$), the flow is strongly accelerated i.e. velocities are increased. As anticipated the case of a solid sphere ($f_w = 0$) falls between the weak suction and weak blowing cases. Peak velocity is located, as in the figures described earlier, at close proximity to sphere surface. With a decrease in blowing and an increase in suction the peaks progressively displace closer to the sphere surface, a distinct effect described in detail in several studies of non-Newtonian boundary layers [41,48,52,53]. Temperature, θ, is also elevated considerably with increased blowing at the sphere surface and depressed with increased suction. The temperature profiles, once again assume a continuous decay from the sphere surface to the free stream, whereas the velocity field initially ascends, peaks and then decays in to the free stream. The strong influence of wall transpiration (i.e. suction or injection) on boundary layer variables is clearly highlighted. Such a mechanism is greatly beneficial in achieving flow control and regulation of heat and mass transfer characteristics in food processing from a spherical geometry.

Figs.13-14, the variation of velocity and temperature fields with different transverse coordinate, ς, is shown. In the vicinity of the sphere surface, velocity f' is found to be maximized closer to the *lower* stagnation point and minimized with progressive distance away from it i.e. the flow is decelerated with increasing ς.

However further from the wall, this trend is reversed and a slight acceleration in the flow is generated with greater distance from the lower stagnation point i.e. velocity values are higher for greater values of ς, as we approach the *upper stagnation point* Temperature θ, is found to noticeably increase through the boundary layer with increasing ς values. Evidently the fluid regime is cooled most efficiently at the lower stagnation point and heated more effectively as we

progress around the sphere periphery upwards towards the upper stagnation point. These patterns computed for temperature and velocity evolution around the sphere surface are corroborated with many other studies including work on non-Newtonian Casson fluid convection by Kandasamy *et al.* [44].

In Figs.15-16, depicts the velocity response to a change in Darcy number, *Da*. This parameter is directly proportional to the permeability of the regime and arises in the linear Darcian drag force term in the momentum equation (9), viz ,$-\frac{f'}{DaGr^{1/2}}$. As such increasing *Da* will serve to reduce the Darcian impedance since progressively less fibers will be present adjacent to the sphere in the porous regime to inhibit the flow. The boundary layer flow will therefore be accelerated and indeed this is verified in Fig.15 where we observe a dramatic rise in flow velocity (f'), with an increase in *Da* from 0.001 through 0.01, 0.1, and 0.2 to 0.5. In close proximity to the sphere surface a velocity shoot is generated; with increasing Darcy number this peak migrates slightly away from the wall into the boundary layer. Evidently lower permeability materials serve to decelerate the flow and this can be exploited in materials processing operation where the momentum transfer may require regulation

In Fig.17 depicts the velocity (f') response for different values of Forchheimer inertial drag parameter (Λ), with radial coordinate (η). The Forchheimer drag force term, $\left(-\xi\Lambda f'^2\right)$ in the dimensionless momentum conservation equation (9) is quadratic and with an increase in Λ (which is in fact related to the geometry of the porous medium) this drag force will increase correspondingly. As such the impedance offered by the fibers of the porous medium will increase and this will effectively decelerate the flow in the regime, as testified to by the evident decrease in velocities shown in Fig. (17). The Forchheimer effect serves to super seed the Darcian body force effect at higher velocities, the latter is dominant for lower velocity regimes and is a linear body force. The former is dominated at lower velocities (the square of a low velocity yields an even lower velocity) but becomes increasingly dominant with increasing momentum in the flow i.e. when inertial effects override the viscous effects (Fig.17).

Fig.18 shows that temperature θ is increased continuously through the boundary layer with distance from the sphere surface, with an increase in Λ, since with flow deceleration, heat will be diffused more effectively via thermal conduction and convection. The boundary layer regime will therefore be warmed with increasing Λ and boundary layer thickness will be correspondingly increased, compared with velocity boundary layer thickness, the latter being reduced.

Figs.19-20, show the effect of velocity slip parameter S_f on sphere surface shear stress (f") and local Nusselt number (-θ') variation. In consistency with

the earlier graphs described for velocity evolution, with an increase in S_f, wall shear stress is consistently reduced i.e. the flow is *decelerated* along the sphere surface. Again this trend has been observed by Wang and Ang [45] and Wang [46] using asymptotic methods. There is also a *progressive migration* in the peak shear stress locations further from the *lower stagnation point*, as wall slip parameter is increased. The impact of wall slip is therefore significant on the boundary layer characteristics of Casson flow from a sphere. With an increasing S_f, the local Nusselt number is also considerably decreased and profiles are generally monotonic decays. Maximum local Nusselt number always arises at the sphere surface and is minimized with proximity to the lower stagnation point i.e. greater distance from the *upper stagnation point*. This pattern of behaviour has also been observed and emphasized by Yih [34] for *Newtonian* flow. In both figures 19 and 20, skin friction coefficient and local Nusselt number are maximized for the case of no-slip i.e. $S_f = 0$, this result concurring with the analyses of Chang [47] and also Hayat *et al.* [48].

Figs.21-22, show the effect of thermal slip parameter S_T on dimensionless wall shear stress function i.e. skin friction coefficient and local Nusselt number, respectively. Increasing S_T is found to decrease both skin friction coefficient and local Nusselt number. A similar set of profiles is computed as in figure 21 for velocity distributions, and we observe that with *increasing thermal slip*, peak velocities are displaced *closer* to the lower stagnation point. For lower values of thermal slip, the plots are also similar to those in figure 22, and have a parabolic nature; however with S_T values greater than 1, the profiles lose their curvature and become increasingly *linear* in nature. This trend is maximized for the highest value of $S_T(= 5.0)$ for which local Nusselt number is found to be almost invariant with transverse coordinate, ξ.

Figs.23-24, illustrate the effect of Casson fluid parameter, β, on skin friction coefficient and local Nusselt number, respectively. With an increase in β the skin friction coefficient increases, since as computed earlier, the flow velocity is enhanced with higher values of β. Larger β values correspond to a progressive decrease in yield stress of the Casson fluid i.e. a reduction in rheological characteristics. With higher β the flow approaches closer to *Newtonian* behaviour and the fluid is able to shear faster along the sphere surface. Local Nusselt number is conversely found to decrease slightly as Casson fluid parameter is increased. This concurs with the earlier computation (fig.8) on temperature distribution. With increasing β values, less heat is transferred from the sphere surface to the fluid regime, resulting in lower temperatures in the regime external to the sphere and lower local Nusselt numbers, as observed in fig.24.

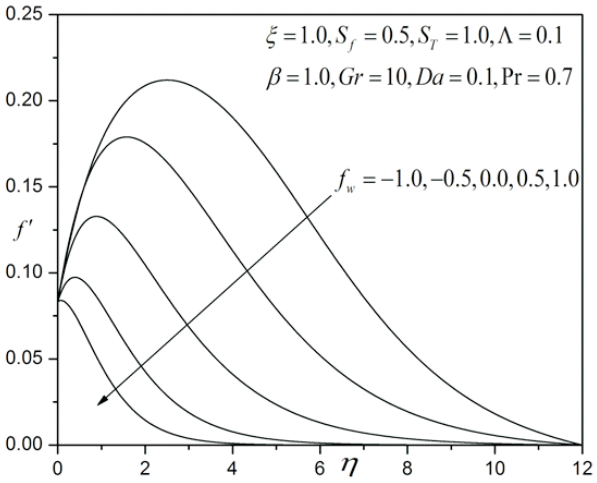

Figure 11: Influence of f_w on velocity profiles

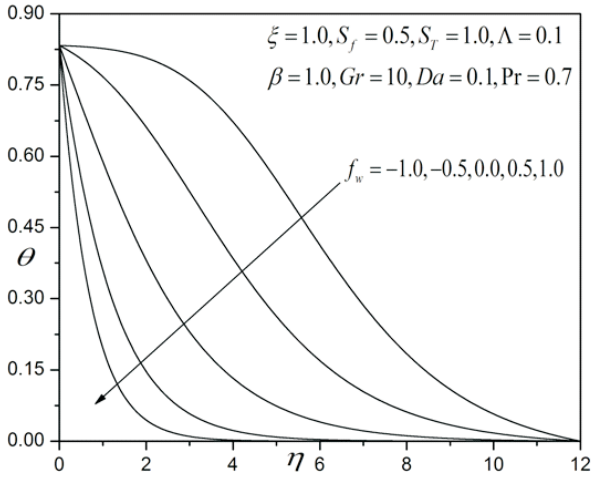

Figure 12: Influence of f_w on temperature profiles

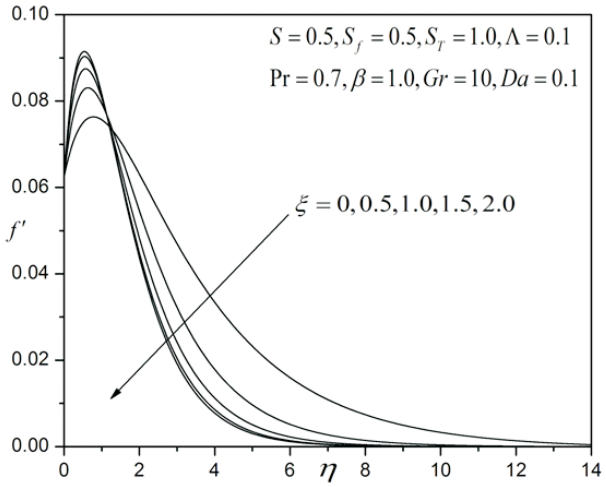

Figure 13: Influence of ξ on velocity profiles

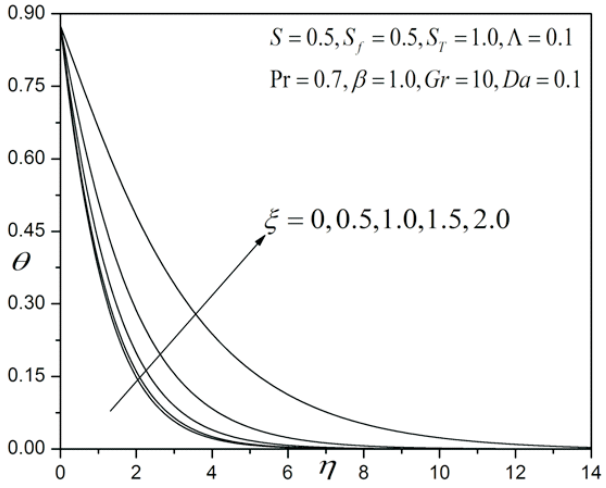

Figure 14: Influence of ξ on temperature profiles

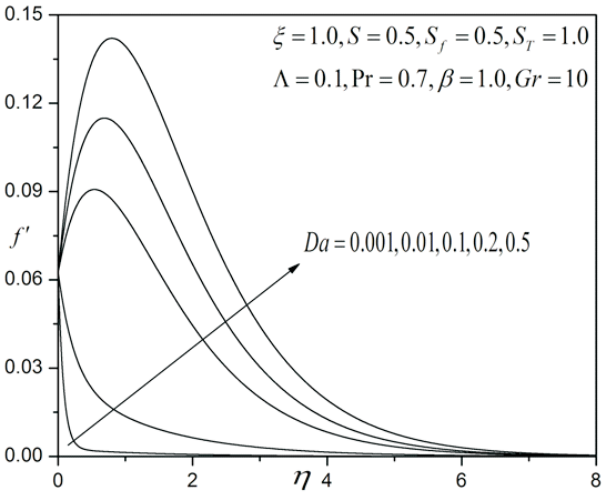

Figure 15: Influence of Da on velocity profiles

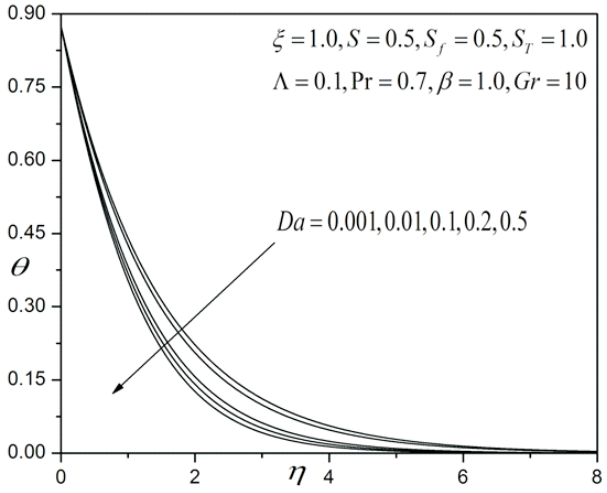

Figure 16: Influence of Da on temperature profiles

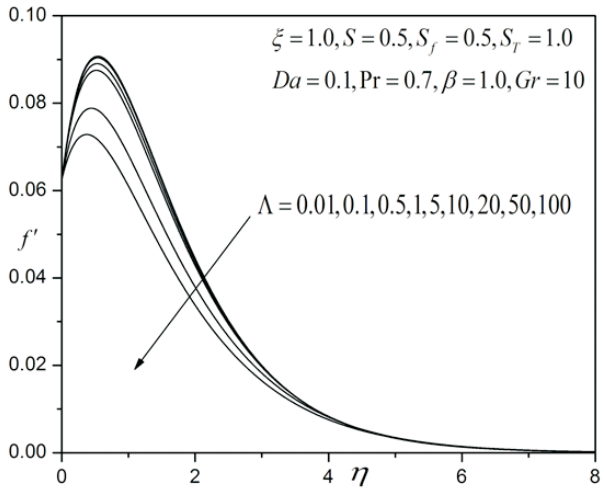

Figure 17: Influence of Λ on velocity profiles

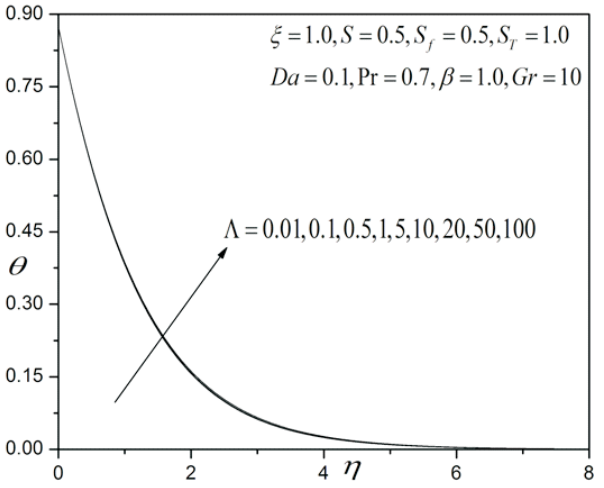

Figure 18: Influence of Λ on temperature profiles

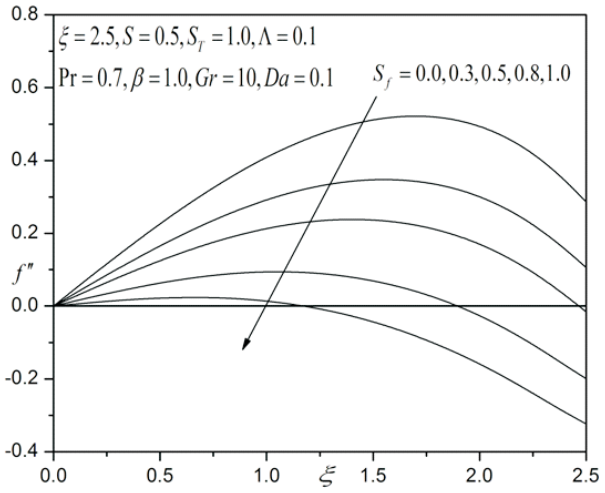

Figure 19: Effect of S_f on the skin-friction coefficient results

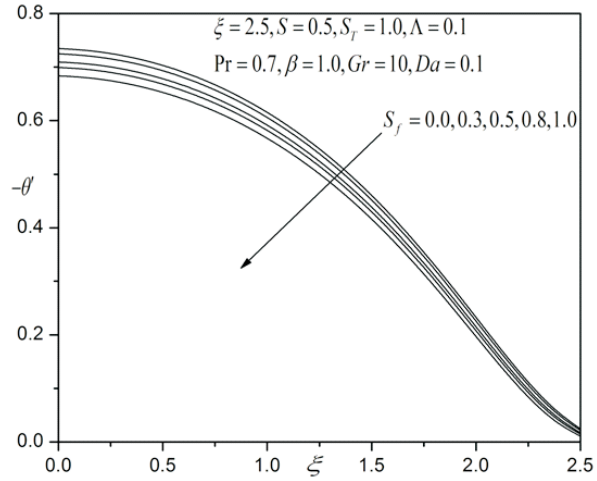

Figure 20: Effect of S_f on the local Nusselt number results

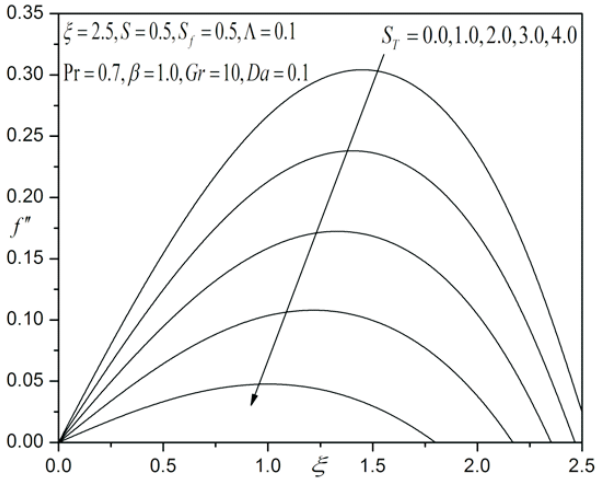

Figure 21: Effect of S_T on the skin-friction coefficient results

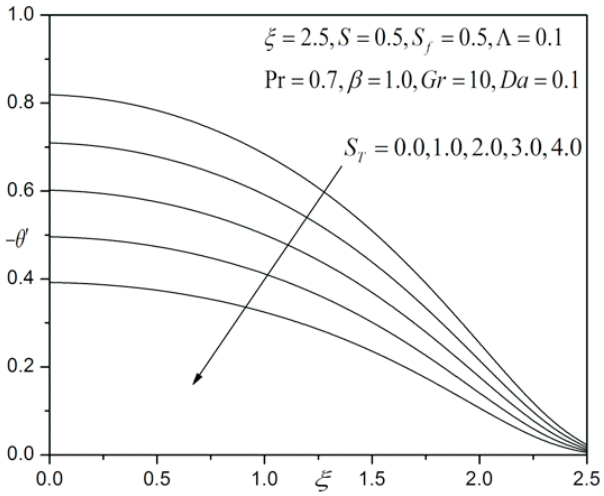

Figure 22: Effect of S_T on the local Nusselt number results

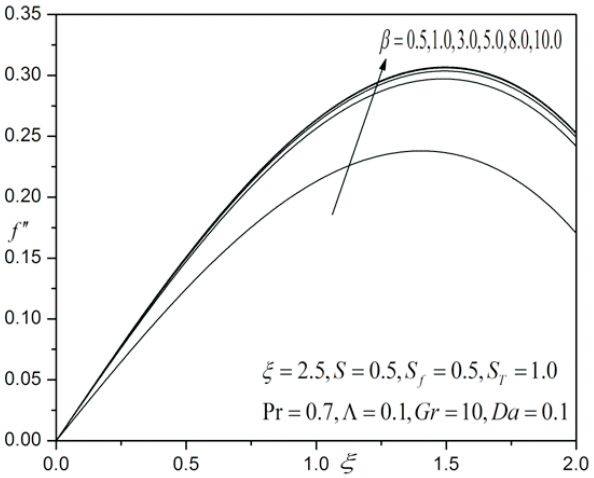

Figure 23: Effect of β on the skin-friction coefficient results

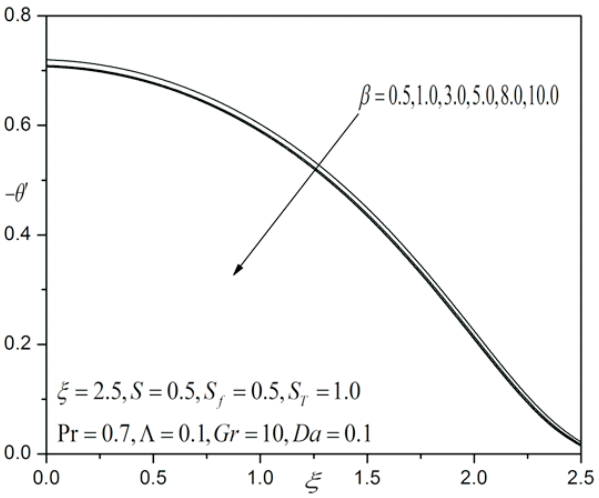

Figure 24: Effect of β on the local Nusselt number results

5 Conclusions

Numerical solutions have been presented for the transport phenomena i.e. combined heat and flow of Casson rheological fluid external to a isothermal sphere, with suction/injection effects and velocity/thermal slip. The model has been developed to simulate foodstuff transport processes in industrial manufacturing operations. A robust, extensively-validated, implicit finite difference numerical scheme has been implemented to solve the transformed, dimensionless velocity and thermal boundary layer equations, subject to physically realistic boundary conditions. The computations have shown that:

1. Increasing the velocity slip parameter, $S_{f,}$ reduces the velocity near the sphere surface and also skin friction coefficient and also increases temperature and decreases local Nusselt number.

2. Increasing the thermal slip parameter, S_T, decreases velocity and skin friction coefficient and also reduces temperature for all values of radial coordinate i.e. throughout the boundary layer regime, and furthermore decreases local Nusselt number.

3. Increasing the Casson fluid parameter,β, increases the velocity near the sphere surface but decreases velocity further from the sphere, and also fractionally lowers the temperature throughout the boundary layer regime.

4. Increasing the Casson fluid parameter, β, strongly increases the wall shear stress (skin friction coefficient) and slightly decreases the local Nusselt number, with the latter more significantly affected at large distances from the lower stagnation point i.e. higher values of transverse coordinate.

5. Increasing Prandtl number, Pr, decelerates the flow and also strongly depresses temperatures, throughout the boundary layer regime.

6. Increasing suction at the sphere surface ($f_w > 0$) decelerates the flow whereas increasing injection ($f_w < 0$, i.e. blowing) induces a strong acceleration.

7. Increasing suction at the sphere surface (f_w ¿0) reduces temperature whereas increasing injection ($f_w < 0$ i.e. blowing) induces the opposite response and elevates temperature.

8. Increasing transverse coordinate, ξ, depresses velocity near the sphere surface but enhances velocity further from the sphere, whereas it continuously increases temperature throughout the boundary layer.

9. The velocity decreases with the increase the non-Darcy parameter and is found to increase the temperature. The velocity increases with the increase the Darcian parameter (Da) and is found to decrease the temperature.

The current study has been confined to steady-state flow i.e. ignored transient effects [49] and also neglected thermal radiation heat transfer effects [50, 51]. These aspects are also of relevance to rheological food processing simulations and will be considered in future investigations.

Acknowledgements

The authors are grateful to the reviewers for their constructive comments which have helped to improve the present article.

References

[1] Schowalter W.R. Mechanics of Non-Newtonian Fluids, **Pergamon Press, USA**,(1978).

[2] Jamil M., Fetecau C., Imran M. Unsteady helical flows of Oldroyd-B fluids, **Commu. Nonlinear Sci. Num. Simu.** Vol.16, pp.1378 – 138 (2011).

[3] Nazar M. , Fetecau C. , Vieru D., Fetecau C. New exact solutions corresponding to the second problem of Stokes for second grade fluids, Nonlinear Analysis: **Real World Appl.** Vol.11, pp.584 – 591 (2010)

[4] Fetecau C. , Hayat T. , Zierep J., Sajid M. Energetic balance for the Rayleigh—Stokes problem of an Oldroyd-B fluid, Nonlinear Analysis: **Real World Appl.**Vol.12, pp.1–13 (2011)

[5] Wang S.W., Tan W.C. Stability analysis of double-diffusive convection of Maxwellfluid in a porous medium heated from below, **Phys. Lett. A .** Vol.372, pp.3046 – 3050 (2008)

[6] Tan W.C., Xu M.Y. Unsteady flows of a generalized second grade fluid with the fractional derivative model between two parallel plates, **Acta Mech.** Sin. Vol.20, pp.471-476 (2004)

[7] Zhang Z.Y. , Fu C.J. , Tan W.C., Wang C.Y. On set of oscillatory convection in a porous cylinder saturated with a viscoelastic fluid, **Phys Fluids**. Vol.19, pp.098 – 104 (2007)

[8] Rashidi M.M , Chamkha A. J., Keimanesh M. Application of multi-step differential transform method on flow of a second grade fluid over a stretching or shrinking sheet, **American J. Comput. Math.** Vol.6, pp.119 - 128 (2011)

[9] Ali N. , Hayat T., Asghar S. Peristaltic flow of Maxwell fluid in a channel with compliant walls, Chaos, Solitons & Fractals. Vol.39, pp.407 - 416 (2009)

[10] Hayat T. , Qasim M. , Abbas Z., Hendi A. A. Magnetohydrodynamic flow and mass transfer of a Jeffery fluid over a nonlinear stretching surface, Z Naturforsch A. Vol.64, pp.1111 - 1120 (2010)

[11] Hussain M. , Hayat T. , Asghar S., Fetecau C. Oscillatory flows of second grade fluid in a porous spac, Nonlinear Analysis**: Real World Appl.** Vol.11, pp.2403 - 2414 (2010)

[12] Dorfman, K. D., Brenner H. 'Generalized Taylor-Aris dispersion in discrete spatially periodic networks: Microfluidic applications', **Phys. Rev. E**., Vol. 65, pp. 20-37 (2002).

[13] Delgado, J.M.P.Q. 'Mass Transfer from a Plane Surface Immersed in a Porous Medium with a Moving Fluid', **IChemE J. Chemical Engineering Research and Design**, Vol. 85, pp. 386-394 (2007).

[14] Minkin, L. 'Thermal diffusion of radon in porous media', Radiation Protection Dosimetry, Vol. 106, pp. 267-272 (2003).

[15] Seo T., Kim H-D., Choi J-H., Chung J. H. 'Mathematical modeling of flow field in ceramic candle filter', **J. Thermal Science,** Vol. 7, pp. 85-88 (1998).

[16] Al-Saffar, Ozturk B. , Hughes R. 'A Comparison of porous and non-porous gas-liquid membrane contactors for gas separation'**, IChemE J. Chemical Engineering Research and Design,** Vol. 75, pp. 685-692 (1997).

[17] Ledvinkova B., F. Keller, J. Kosek and U. Nieken. 'Mathematical modeling of the generation of the secondary porous structure in a monolithic adsorbent', **Chemical Engineering J.,** Vol. 140, pp. 578-585 (2008).

[18] Turner I.W., J.R. Puiggali and W. Jomaa. 'A numerical investigation of combined microwave and convective drying of a hygroscopic porous material: a study based on pine wood', **IChemE J. Chemical Engineering Research and Design**, Vol. 76, pp 193-209 (1998).

[19] Pomes V., A. Fernandez and D. Houi. 'Characteristic time determination for transport phenomena during the electrokinetic treatment of a porous medium', **Chemical Engineering J.,** Vol. 87, pp. 251-260 (2002).

[20] Islam M.R.' Route to chaos in chemically enhanced thermal convection in porous media', **Chemical Engineering Communications**, Vol. 124, pp. 77-95 (1993).

[21] Albusairi B. and J. T. Hsu. 'Flow through beds of perfusive particles: effective medium model for velocity prediction within the perfusive media', **Chemical Engineering J.,** Vol. 100, pp. 79-84 (2004).

[22] Khachatoorian R. and Teh Fu Yen.' Numerical modeling of in situ gelation of biopolymers in porous media',[1]. **J. Petroleum Science and Engineering**, Vol. 48, pp. 161-168 (2005).

[23] Casson N. In Reheology of Dipersed system, Peragamon press, Oxford (1959).

[24] M. Nakamura and T.Sawada, Numerical study on the flow of a non-Newtonian fluid through an axisymmetric stenosis**. ASME J. Biomechanical Eng**.Vol.110,pp.137-143 (1988)

[25] R.B.Bird, G. C. Dai, and B. J. Yarusso, The rheology and flow of viscoplastic materials, **Rev.Chem.Eng,** Vol.1, pp.1 – 83 (1983)

[26] C. Derek, D. C. Tretheway and C. D. Meinhart, Apparent fluid slip athydrophobic microchannel walls**, Phy. Fluids**. Vol.14, pp.1 – 9 (2002).

[27] Nield,D.A and Bejan, A., convection in porous media, third ed., **springer, Newyork**(2006)

[28] Keller, H.B. A new difference method for parabolic problems, J. Bramble (Editor), **Numerical Methods for Partial Differential Equations** (1970).

[29] V.Ramachandra Prasd, B.Vasu and O.Anwer Bég.'Thermo-Diffusion and Diffusion-Thermo effects on boundary layer flows',**LAP LAMBERT Academic Publishing GmbH & co.KG,Dudwelier andstr.99,66123 Saarbrucken, Germany** (2011).

[30] V.Ramachandra Prasd, B.vasu and O.Anwer Bég 'Thermo-diffusion and diffusion-thermo effects on MHD free convection flow past a vertical porous plate embedded in a non-Darcian porous medium' **Chemical Engineering Journal** Vol.173, pp.598–606(2011)

[31] O. Anwar Bég , V. Ramachandra Prasad, B. Vasu , N. Bhaskar Reddy , Q. Li , R. Bhargava Free convection heat and mass transfer from an isothermal sphere to a micropolar regime with Soret/Dufour effects **International Journal of Heat and Mass Transfer** ' Vol.54, pp.9–18 (2011)

[32] Cebeci T., Bradshaw P., Physical and Computational Aspects of Convective Heat Transfer, **Springer, New York** (1984).

[33] H.B. Keller, A new difference method for parabolic problems, ***J. Bramble (Editor), Numerical Methods for Partial Differential Equations, Academic Press, New York, USA*** (1970).

[34] K.A. Yih, Effect of blowing/suction on MHD-natural convection over horizontal cylinder: UWT or UHF, ***Acta Mechanica***, 144, 17-27 (2000).

[35] Merkin, J.H., Free convection boundary layers on cylinders of elliptic cross section. **J. heat transfer,** 99 (1977) 453-457.

[36] L. J. Crane and A. G. McVeigh, Uniform slip flow on a cylinder, ***PAMM: Proc. Appl. Math. Mech.*** 10, 477478 (2010)

[37] S. O. Ajadi, A. Adegoke and A. Aziz, Slip boundary layer flow of non-Newtonian fluid over a flat plate with convective thermal boundary condition, ***Int. J. Nonlinear Science***, 8, 300-306 (2009).

[38] A. Aziz, Hydrodynamic and thermal slip flow boundary layers over a flat plate with constant heat flux boundary condition, ***Communications in Nonlinear Science and Numerical Simulation***, 15, 573-580 (2010).

[39] F.E. Larrode, C. Housiadas, Y. Drossinos, Slip-flow heat transfer in circular tubes, ***Int. J. Heat Mass Transfer***, 43, 2669-2680 (2000)

[40] H. Attia and M. E. Sayed-Ahmed, Transient MHD Couette flow of a Casson fluid between parallel plates with heat transfer, ***Italian J. Pure Applied Mathematics***, 27, 19-38 (2010).

[41] M. Mustafa, T. Hayat, I. Pop and A. Aziz, Unsteady boundary layer flow of a Casson fluid due to an impulsively started moving flat plate, ***Heat Transfer-Asian Research***, 40, 563–576 (2011)

[42] J.F. Steffe, ***Rheological methods in Food Process Engineering***, 2^{nd} edn, Freeman Press, Michigan, USA (2001).

[43] F. Debaste Y. Kegelaers, H. Ben Hamor and V. Halloin Contribution to the modelling of chocolate tempering, ***Proc. European Congress of Chemical Engineering (ECCE-6), Copenhagen, Denmark, 16-20 September*** (2007).

[44] A. Kandasamy, Karthik. K., Phanidhar P. V., Entrance region flow heat transfer in concentric annuli for a Casson fluid, ***Int. Conf. Thermal Issues in Emerging Technologies, Theory and Application (ThETA), Cairo, Egypt, January 3^{rd}- 6^{th}*** (2007).

[45] C.Y.Wang and C-O. Ng, Slip flow due to a stretching cylinder, ***Int. J. Non-Linear Mechanics***, 46, 1191-1194 (2011).

[46] C.Y. Wang, Stagnation flow on a cylinder with partial slip—an exact solution of the Navier–Stokes equations, ***IMA J. Applied Mathematics***, 72, 271-277 (2007).

[47] T. B. Chang, A. Mehmood, O. Anwar Bég, M. Narahari, M. N. Islam and F. Ameen, Numerical study of transient free convective mass transfer in a Walters-B viscoelastic flow with wall suction, ***Communications in Nonlinear Science and Numerical Simulation***, 16, 216–225 (2011).

[48] T. Hayat, I. Pop and A. A. Hendi, Stagnation-point flow and heat transfer of a Casson fluid towards a stretching sheet, ***Zeit. Fr. Natur.***, 67, 70-76 (2012).

[49] V.R. Prasad, B. Vasu, O.Anwar Bég and R. Parshad, Unsteady free convection heat and mass transfer in a Walters-B viscoelastic flow past a semi-infinite vertical plate: a numerical study,***Thermal Science-International Scientific J., 15, 2, S291-S305 (2011).***

[50] V. R. Prasad, B. Vasu, O. Anwar Bég and D. R. Parshad, Thermal radiation effects on magnetohydrodynamic free convection heat and mass transfer from a sphere in a variable porosity regime, ***Communications in Nonlinear Science and Numerical Simulation,*** 17, 654–671 (2012).

[51] V.R. Prasad, B. Vasu, R. Prashad and O. Anwar Bég, Thermal radiation effects on magneto-hydrodynamic heat and mass transfer from a horizontal cylinder in a variable porosity regime, ***J. Porous Media,*** 15, 261-281 (2012).

[52] O. Anwar Bég, K. Abdel Malleque and M.N. Islam, Modelling of Ostwald-deWaele non-Newtonian flow over a rotating disk in a non-Darcian porous medium, ***Int. J. Applied Mathematics and Mechanics,*** 8, 46-67 (2012).

[53] M.M. Rashidi, O. Anwar Bég and M.T. Rastegari, A study of non-Newtonian flow and heat transfer over a non-isothermal wedge using the Homotopy Analysis Method, ***Chemical Engineering Communications,*** 199, 231-256 (2012).

Submitted in August 2012, revised in July 2013

Modeliranje pojave laminarnog transporta u Casson-ovom reološkom fluidu iz neke izotermske sfere sa delimičnim klizanjem nedarsijevskoj poroznoj sredini

Razmatra se protok i prenos toplote na Casson-tečnosti iz propustljive izotermske sfere u prisustvu klizanja u nedarsijevskoj poroznoj sredini. Površina sfere se održava na konstantnoj temperaturi. Granični sloj jednačine konzervacije, koji je paraboličan u prirodi, je normalizovan u ne-sličnoj formi, a onda rešen brojčano pomoću dobro testirane efikasne, implicitno stabilne, šeme Keller-boks konačnih razlika . Nadjeno je da povećanje parametra brzine klizanja dovodi do smanjenja brzine i debljine graničnog sloja, a do povećanja temperature. Brzina opada sa porastom nedarsijevskog parametra što povećava temperaturu.Brzina raste sa povećanjem Casson-ovog parametra tečnosti i to smanjuje temperaturu. Koeficijent trenja u sloju i lokalni Nusselt-ov broj se po redu smanjuju sa povećanjem brzine i parametra termičkog klizanja.

doi:10.2298/TAM1304469P Math. Subj. Class.: 74S20; 76A05; 76D10; 82D15.